

# Effect of Mg Addition on the Refinement and Homogenized Distribution of Inclusions in Steel with Different Al Contents



LINZHU WANG, SHUFENG YANG, JINGSHE LI, SHUO ZHANG, and JIANTAO JU

To investigate the effect of Mg addition on the refinement and homogenized distribution of inclusions, deoxidized experiments with different amounts of aluminum and magnesium addition were carried out at 1873 K (1600 °C) under the condition of no fluid flow. The size distribution of three-dimensional inclusions obtained by applying the modified Schwartz–Saltykov transformation from the observed planar size distribution, and degree of homogeneity in inclusion dispersion quantified by measuring the inter-surface distance of inclusions, were studied as a function of the amount of Mg addition and holding time. The nucleation and growth of inclusions based on homogeneous nucleation theory and Ostwald ripening were discussed with the consideration of supersaturation degree and interfacial energy between molten steel and inclusions. The average attractive force acted on inclusions in experimental steels was estimated according to Paunov's theory. The results showed that in addition to increasing the Mg addition, increasing the oxygen activity at an early stage of deoxidation and lowering the dissolved oxygen content are conducive to the increase of nucleation rate as well as to the refinement of inclusions. Moreover, it was found that the degree of homogeneity in inclusion dispersion decreases with an increase of the attractive force acted on inclusions, which is largely dependent on the inclusion composition and volume fraction of inclusions.

DOI: 10.1007/s11663-017-0915-y

© The Minerals, Metals & Materials Society and ASM International 2017

## I. INTRODUCTION

NONMETALLIC inclusions are unavoidable during the steelmaking process, and the residue inclusions are frequently reported as the origins of steel performance issues such as fracture and fatigability.<sup>[1–3]</sup> Although much effort has been made in the utmost removal of inclusions, they still exist in products.<sup>[4–9]</sup> In contrast, the idea of using fine oxide inclusions as the heterogeneous nucleation sites has been brought to the forefront with the development of oxide metallurgy. It is proposed that the small oxide inclusions with homogenized distribution can induce intragranular ferrite effectively, which will improve the performance of steel.<sup>[10,11]</sup>

Aluminum is commonly applied as a deoxidizer in the modern steelmaking process due to its strong deoxidation ability and low price. Nevertheless, the generated Al<sub>2</sub>O<sub>3</sub> inclusions tend to aggregate and form large clusters in the molten steel. These inclusions are detrimental to the mechanical properties of products and easily cause nozzle clogging.<sup>[12,13]</sup> Therefore, calcium

treatment is widely used to modify solid Al<sub>2</sub>O<sub>3</sub> inclusions into low-melting calcium aluminates, which is an effective method to prevent the inclusions from clogging the nozzles.<sup>[14–16]</sup> Yet, residual calcium aluminates with a large size have been still detected in products.<sup>[17,18]</sup> Hence, steelmakers were attempting to find new ways to solve this problem,<sup>[19–21]</sup> and it is found that Mg treatment has a remarkable improvement on the steel performance.<sup>[22]</sup> Many scholars advocated that the positive effects of Mg addition in the steel are attributable to the evenly distributed MgO-containing inclusions, and it can be concluded to three points: (1) The generated MgO-containing inclusions present a much weaker tendency to form clusters, and they can prevent the aggregation of aluminum inclusions by forming around their periphery.<sup>[23,24]</sup> (2) Numerous inclusions with small size precipitate in the steel with Mg treatment. Jiang *et al.* observed that inclusions decreased from 1.91 to 1.29 μm and the number density increased from  $2.96 \times 10^4$  to  $5.62 \times 10^4$  mm<sup>-3</sup> in the steel with the addition of Mg, compared with the steel without Mg addition.<sup>[25]</sup> (3) The fine MgO-containing inclusions have a facilitating effect on the formation of equiaxed crystallization and refinement of microstructure.<sup>[26–28]</sup> The experimental research indicates that the finer the inclusion particle is and the more the unit volume number is, the stronger the pinning effect is and the finer the grain is.<sup>[25]</sup> These studies indicate that it is of crucial importance to obtain numerous

LINZHU WANG, SHUFENG YANG, JINGSHE LI, and SHUO ZHANG are with the School of Metallurgical and Ecological Engineering, University of Science and Technology Beijing, Beijing 100083, P.R. China. JIANTAO JU is with the School of Metallurgical and Ecological Engineering, Xi'an University of Architecture and Technology, Xi'an 710055, P.R. China. Contact e-mail: yangshufeng@ustb.edu.cn

Manuscript submitted August 26, 2016.

Article published online February 1, 2017.

MgO-containing inclusions with small size and uniform distribution.

In the view of controlling size and number of inclusions, the nucleation and growth of inclusions during the deoxidation process in the steel must be considered. The calculation results of Zhang *et al.*<sup>[29,30]</sup> based on thermodynamic analysis and numerical simulation indicate that the inclusion nuclei is predicted to be about 10 to 20 Å in diameter and nucleation is very fast, occurring predominantly between 1 and 10 milliseconds. Suito and Ohta *et al.*<sup>[31–33]</sup> investigated the growth mechanism of deoxidation products under the condition of no melting stirring. They discussed the size and number of inclusions as a function of time based on diffusion growth, coagulation due to the difference in ascending velocity, and the coagulation due to Brown motion and the coarsening by Ostwald ripening, and they concluded that Ostwald growth is the predominate mechanism under the condition of no melting stirring.<sup>[31]</sup> Moreover, it is found that the nucleation and growth of inclusions are affected by the interfacial energy between inclusions and steel, the amount and kind of deoxidizer, and the content of oxygen.<sup>[31–33]</sup> On the other hand, for controlling the dispersion of inclusions in the steel, the behavior of inclusions was mainly discussed in terms of the holding time, cooling rate, and composition of inclusions.<sup>[34–36]</sup> Kimura *et al.*<sup>[24]</sup> studied the aggregation of inclusions in the molten steel and evaluated the attractive force acted on inclusions semiquantitatively with the application of Paunov's theory and proposed that the attractive force is dependent on the interfacial energy between inclusions with steel and the distance between inclusions. It can be concluded that the steel composition and chemistry of inclusions have great influence on the behavior of inclusions.

Considerable experimental research has been aimed at the thermodynamics on the formation of magnesium aluminate spinel in the liquid steel.<sup>[37–41]</sup> Nonetheless, there are limited reports on the behavior of MgO-containing inclusions in high-temperature molten steel, especially the homogeneity of inclusion distribution, which affects the pinning effect directly. In the present study, the effect of Mg addition on the size, number of three-dimensional inclusions, distribution of area density of inclusions, and degree of homogeneity in inclusion dispersion were studied systematically in the steel with different Al contents. The influencing factors for obtaining numerous fine and uniform dispersed inclusions were analyzed based on homogeneous nucleation theory, Ostwald ripening, and Paunov's theory. The current study will be helpful to solve the problems about aggregation and coarsening of inclusions in the steel.

## II. EXPERIMENTAL

### A. Procedure

The Si-Mo heating electric resistance furnace was used for melting experiments. A total of 600 g of steel material as shown in Table I was enclosed in the Al<sub>2</sub>O<sub>3</sub>

crucible (56 mm OD × 50 mm ID × 100 mm HT) before it was set at the even temperature zone of the Al<sub>2</sub>O<sub>3</sub> reaction tube. The melt was heated to 1873 K (1600 °C) and was held for 30 minutes under Ar gas flowing atmosphere (5 L/min) to make the steel molten and homogenized completely. Then, the Al powder (>99 pct Al) and Ni-17 wt pct Mg alloy packed in iron foil were added and immediately the melt was stirred by a molybdenum rod for 10 s to disperse the primary inclusions uniformly. To investigate the effect of Mg addition on the behavior of inclusions in the steel with different Al contents, [pct Mg]<sub>i</sub> = 0, 0.03, 0.1 (*i* represents the initial addition of a deoxidant) was added in the steel with [pct Al]<sub>i</sub> = 0.05, 0.25, and 0.55 as shown in Table II.

The steel samples were taken by a quartz tube (6 mm ID) at 120, 600, 1800, and 3900 seconds after deoxidizer addition, followed by quenching in salt water. Before being inserted into the molten steel, the quartz tube was injected with Ar gas to prevent reoxidation of steel samples. Considering the depth of liquid steel, which was about 40 mm for 600 g of steel material reduced 2 mm at each sampling, the sampling location was set at 15 mm from the bottom of the crucible and the quartz tube was marked with the red line to record the distance from the bottom of crucible to the top of the Al<sub>2</sub>O<sub>3</sub> tube. The length of samples was controlled as 150 mm (33 g) by connecting the quartz tube with a syringe. In addition, to keep the same initial condition in all the experiments, the oxygen content was measured before deoxidizer addition and they were about 200 ± 20 mass ppm (ppm represents mass ppm).

### B. Chemical Analysis

The total oxygen content in the samples was determined by fusion-infrared absorption, and each sample was measured three times. Soluble Al and total Mg content in steel were analyzed by the ICP-AES method. As the insoluble element presents as oxide inclusions in the steel, it can be estimated as Eq. [1]. Furthermore, FACTSAGE 7.0 was used to calculate the soluble element content at equilibrium:

$$[\text{pct O(M)}]_{\text{Insol.}} = f_V \cdot \frac{\rho_{\text{M}_x\text{O}_y}}{\rho_{\text{Fe}}} \cdot \frac{yM_{\text{O}}(xM_{\text{M}})}{M_{\text{M}_x\text{O}_y}} \times 10^6 \quad [1]$$

where  $f_V$  is the total volume fraction of oxide inclusions,  $\rho_{\text{Fe}}$  is the density of Fe, and  $\rho_{\text{M}_x\text{O}_y}$  is the density of the oxide inclusions ( $\rho_{\text{Fe}} = 7.8 \text{ g/cm}^3$ ,  $\rho_{\text{Al}_2\text{O}_3} = 3.97 \text{ g/cm}^3$ ,  $\rho_{\text{MgO}} = 3.65 \text{ g/cm}^3$ ).  $\rho_{\text{Al}_2\text{O}_3\text{-MgO}} = X_{\text{Al}_2\text{O}_3} \cdot \rho_{\text{Al}_2\text{O}_3} + X_{\text{MgO}} \cdot \rho_{\text{MgO}}$ .  $M_{\text{M}_x\text{O}_y}$  and  $X_{\text{M}_x\text{O}_y}$  is the molecular weight of  $\text{M}_x\text{O}_y$  and the molar fraction of  $\text{M}_x\text{O}_y$ .<sup>[33]</sup>

### C. Measurement and Estimation of Inclusions

The specimens were machined into a semicylinder through their maximum longitudinal section to analyze characteristics of inclusions at horizontal and vertical directions, and a longitudinal section (Φ6 mm × 15 mm)

**Table I. Chemical Composition of Steel Material (Weight Percent)**

Element	C	Si	Mn	P	S	Cr	Als	Cu	Ni	Ti	N
Content	0.0016	0.0033	0.01	0.0053	0.0017	0.0107	0.003	0.0037	0.0038	0.001	0.0020

**Table II. Chemical Composition of Metal, Volume Fraction of Inclusions, and Average Minimum Intersurface Distance Between Inclusions**

Exp. No	Deoxidant	Holding time at 1873 K (1600 °C) (s)	[O]		[Al]		[Mg]		Insol. (Mass ppm)	Sol. (Mass ppm)	Insol. (Mass ppm)	Sol. (Mass ppm)	$V_f$ (10 <sup>-4</sup> )	$\overline{D_A}$
			Total (Mass ppm)	Sol. (Mass ppm)	Sol. (Mass ppm)	Insol. (Mass ppm)	Sol. (Mass ppm)	Insol. (Mass ppm)						
A1	0.05pctAl	3900	8.3 to 117.0	3.8*	220	208.9	—	—	7.8	17	—	—	7.8	17
A1M1	0.05pctAl + 0.03pctMg	3900	37.3 to 40.6	3.4*	250	38.8	0.02*	9.9	1.8	51	—	—	1.8	51
A1M2	0.05pctAl + 0.1pctMg	3900	42.7 to 43.5	1.2*	230	32.2	0.05*	21.4	2.0	61	—	—	2.0	61
A2	0.25pctAl	120	186.9 to 188.9	1.5 to 4.4	1800	210.8	—	—	7.9	12	—	—	7.9	12
		600	128.8 to 130	0.9* to 5.6	1900	140.0	—	—	5.2	19	—	—	5.2	19
		1800	53 to 71.3	0.9* to 2.5	1800	77.4	—	—	2.9	25	—	—	2.9	25
		3900	23.9 to 24.6	0.9*	1800	31.3	—	—	1.1	53	—	—	1.1	53
A2M1	0.25pctAl + 0.03pctMg	120	155.1 to 162.2	0.9 to 2.4	2100	174.2	7.5	2.5	6.8	12	—	—	6.8	12
		600	119.0 to 119.3	0.8*	2200	148.0	8.4	6.8	5.7	17	—	—	5.7	17
		1800	60.0 to 180.3	0.8* to 60	2100	115.8	0.1*	26.5	5.3	15	—	—	5.3	15
		3900	38.0 to 93.5	0.8*	2100	93.0	0.1*	17.5	4.0	21	—	—	4.0	21
A2M2	0.25pctAl + 0.1pctMg	120	137.3 to 146.1	1.0 to 1.8	1400	117.6	11.1	33.9	7.1	10	—	—	7.1	10
		600	110.6 to 179.9	0.4* to 8.9	1500	131.3	0.2*	103.6	7.9	12	—	—	7.9	12
		1800	64.9 to 90.8	0.4* to 1.8	1400	50.9	0.2*	26.8	2.8	28	—	—	2.8	28
		3900	34.6	0.4* to 3.1	1400	26.4	0.2*	12.0	1.4	60	—	—	1.4	60
A3	0.55pctAl	3900	20.6 to 21.9	0.4*	4900	25.6	—	—	1.0	79	—	—	1.0	79
A3M1	0.55pctAl + 0.03pctMg	3900	48.9 to 50.9	0.4*	5200	49.9	0.2*	9.6	2.2	32	—	—	2.2	32
A3M2	0.55pctAl + 0.1pctMg	3900	36.3	0.2*	5300	31.8	0.5*	13.8	1.6	56	—	—	1.6	56

$V_f$  presents volume fraction of inclusions.

was wet grinding to 2000 grit followed by diamond polishing. The chemical composition of oxide inclusions was detected by SEM-EDS. The continuous 169 SEM microphotographs were taken at a magnification of 1000 corresponding to the total area of 3.5 mm × 3.5 mm. Considering a larger observed area is needed for inclusions with nonuniform distribution, before taking the SEM microphotographs, the sample was scanned entirely to see the distribution of inclusions. The dividing line was marked between the region with concentrated inclusions and that with dispersed inclusions for nonuniform distributed inclusions. Successive 169 SEM microphotographs (13 × 13) were taken in each region (total number of SEM microphotographs is 338 in the sample with nonuniform distributed inclusions). In addition, the planar size, number, and central coordinates of inclusions were analyzed by Image-Pro-Plus software. As the limitation of resolution, there are statistical and systematic measurement errors in the detection of small inclusions; therefore, the inclusions no more than 200 nm have not been analyzed.

1. Number and size of three-dimensional inclusions

Saltykov modified the Schwartz–Saltykov (SS) method<sup>[42]</sup> by introducing the probability mass function (PMF), which makes transformation from two-dimensional spherical inclusions size distribution to

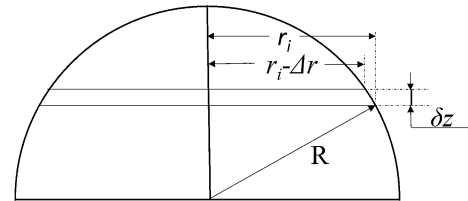


Fig. 1—Intersecting cross section of spherical inclusion.

three-dimensional inclusions size distribution more accurate. As shown in Figure 1, most inclusions in the metallographic samples are not sectioned through their maximum cross section and the probability of a cross section with radius  $r$  ( $r_i - \Delta r < r < r_i$ ) intersecting a sphere with radius  $R$  is given by:<sup>[43]</sup>

$$P(r/R) = \frac{\delta z}{R} = \frac{1}{R} (\sqrt{(R^2 - (r_i - \Delta r)^2)} - \sqrt{R^2 - r_i^2}) \quad [2]$$

Based on the measured mean radius of inclusions in two-dimensions, they were classified into 49 successive groups from the largest inclusions (the diameter of largest inclusions in all samples is no more than 19.6 μm) to the smallest ones and an interval of groups is 0.2 μm in this study. Therefore, the radius of inclusions in group 1 denoted by  $r = 9.8 \mu\text{m}$  or by  $d = 19.6 \mu\text{m}$  is in

the range of 9.7 to 9.9  $\mu\text{m}$ , group 2 is denoted by  $r = 9.6 \mu\text{m}$ , and group 49 is denoted by  $r = 0.2 \mu\text{m}$ . According to the literature of Saltykov<sup>[42]</sup> and Li,<sup>[43]</sup> the detected two-dimensional inclusions in group  $j$  probably belongs to the three-dimensional group  $i$ , which has larger inclusions ( $i \leq j$ ) as expressed as Eq. [3], where  $N_A$  and  $N_V$  are the number of inclusions in two-dimensional and three-dimensional, respectively. The transformation from two-dimensional spherical inclusions size distribution to three-dimensional inclusions size distribution can be performed by Eqs. [4] and [5] is the  $P$  matrix ( $P^{-1}$  is the inverse matrix of the  $P$  matrix):

$$N_A(j) = \sum_{i=1}^j d_i N_V(i) P(j, i) \quad [3]$$

$$\begin{bmatrix} d_1 N_V(1) \\ d_2 N_V(2) \\ d_3 N_V(3) \\ \vdots \\ d_n N_V(n) \end{bmatrix} = P^{-1} \begin{bmatrix} N_A(1) \\ N_A(2) \\ N_A(3) \\ \vdots \\ N_A(n) \end{bmatrix} \quad [4]$$

$$\begin{bmatrix} P(1,1) \\ P(2,1) & P(2,2) \\ P(3,1) & P(3,2) & P(3,3) \\ P(4,1) & P(4,2) & P(4,3) & P(4,4) \\ P(5,1) & P(5,2) & P(5,3) & P(5,4) & P(5,5) \\ \dots & \dots & \dots & \dots & \dots & \dots \\ P(n,1) & P(n,2) & P(n,3) & \dots & \dots & P(n,n-1) & P(n,n) \end{bmatrix} \quad [5]$$

To apply this method to the transformation of non-spherical particles, Li<sup>[43]</sup> proposed that the PMF of nonspherical particles can be obtained by measuring their fractal dimension. Nevertheless, it is difficult to detect or estimate the fractal dimension of each inclusion in this study. The roundness of inclusions are measured by Image-ProPlus, and they are mostly in the range of 1 to 1.7, indicating that inclusions in this study are near-spherical. Therefore, the number, size, and volume fraction of inclusions in three-dimensional were obtained by treating the  $\text{Al}_2\text{O}_3$  and  $\text{Al}_2\text{O}_3\text{-MgO}$  as a sphere with Eqs. [2] to [5], and then the insoluble oxygen content can be calculated based on Eq. [1]. The results of calculated oxygen content and observed oxygen content are compared in Figure 2, and the observed value is the average value of oxygen content measured three times in each sample. There is a good correspondence in the cases with homogenous distribution of oxygen but not in the cases with nonuniform distribution of oxygen. This finding suggests that the measurement of inclusion size and number by SEM microphotographs is well established and that the modified SS method is well applied.

#### D. Minimum Intersurface Distance

The intersurface distance between the two particles is given by:

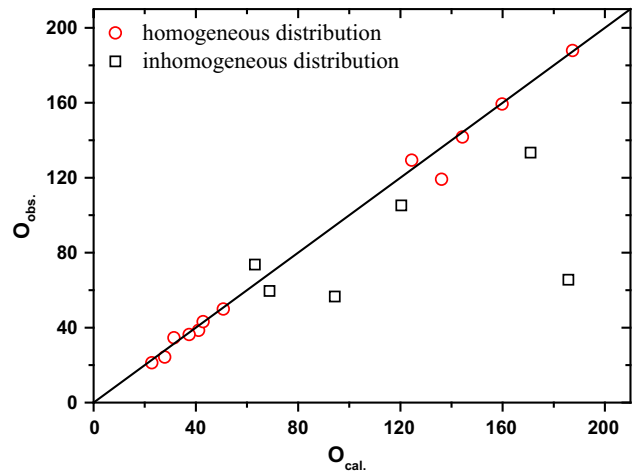


Fig. 2—Comparison of observed oxygen content and calculated oxygen content.

$$D_{ab} = \sqrt{(X_b - X_a)^2 + (Y_b - Y_a)^2} - r_a - r_b \quad [6]$$

where  $X_i$  and  $Y_i$  are the central coordinates of inclusions in the cross section,  $r_i$  is the equivalent radius, and  $D_{ab}$  is the intersurface distance between two inclusions. A minimum intersurface distance of a certain inclusion is the intersurface distance between this inclusion and its nearest inclusion, which can be obtained by:

$$D_{m_i} = \text{MIN}(D_{i1}, D_{i2}, \dots, D_{ik}) \quad [7]$$

### III. RESULTS

#### A. Inclusion Composition

It was confirmed from SEM-EDS analysis that the compositions of deoxidation products with Al and Al-Mg were  $\text{Al}_2\text{O}_3$  and  $\text{Al}_2\text{O}_3\text{-MgO}$  complex inclusions, respectively. According to the  $\text{Al}_2\text{O}_3\text{-MgO}$  phase diagram at 1873 K (1600 °C),<sup>[44]</sup> inclusions exist as  $\text{Al}_2\text{O}_3 + \text{spinel}$ ,  $\text{spinel}$ , and  $\text{spinel} + \text{MgO}$  when MgO is below 16 pct, in the range 16 to 28 pct and above 28 pct, respectively. Figure 3 presents the composition of inclusions in the steel after Mg addition at 3900 seconds, which indicates that the MgO content in the inclusions increases with the increasing amount of Mg addition in the steel. According to the inclusion composition, the experiments can be classified into three groups, *i.e.*, A2M1 and A3M1 with inclusions containing mainly  $\text{Al}_2\text{O}_3 + \text{spinel}$  complex phases; A1M1, A2M2, and A3M2 with inclusions mainly isolated  $\text{spinel}$ -only phase; and A1M2 with inclusions mainly  $\text{spinel} + \text{MgO}$  complex phases. There were also some  $\text{spinel} + \text{MgO}$  containing inclusions left in Exp. A2M2 and Exp. A3M2, and isolated  $\text{MgO}$ -only containing inclusions were observed in Exp. A3M1.

The evolution of inclusion composition in the steel with different Mg additions is shown in Figure 4. The error bars represent the range between the maximum



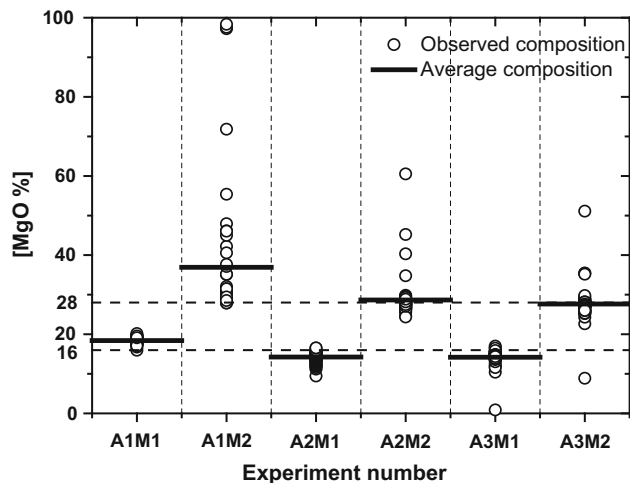


Fig. 3—Composition of inclusions in steel with Mg addition.

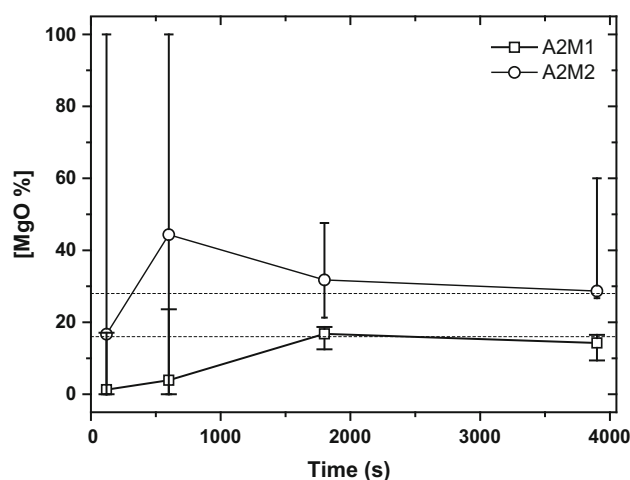


Fig. 4—Change of MgO content of inclusions with holding time.

and the minimum MgO content of inclusions. The inclusions almost all precipitated as  $\text{Al}_2\text{O}_3$  + spinel phases in the experiment with initial deoxidant of  $[\text{pct Mg}]_i = 0.03$  and the MgO content kept increasing during the first 1800 seconds. In the case with an initial deoxidant of  $[\text{pct Mg}]_i = 0.1$ , the isolated MgO-only inclusions generated during the first 600 seconds.

## B. Inclusion Characteristics

### 1. Size distribution of three-dimensional inclusions

Figure 5 shows the size distribution of three-dimensional inclusions in the steel containing different Al and Mg contents at the holding time of 3900 seconds at 1873 K (1600 °C). Some points are deviated from the fitted curve slightly due to the effect of inclusion shape or division of the classes probably. The fitted curves as shown in Figure 5 can reflect the distribution regulation of the measurement data by performing an error analysis. The shape of curves becomes narrower and higher with the addition of Mg regularly, which

indicates more fine inclusions precipitated in the steel with Mg treatment. The curves of Exp. A1M1, Exp. A2M1, and Exp. A3M1 have the highest peak, suggesting that there were a large number of inclusions in the experiments with an initial deoxidant of  $[\text{pct Mg}]_i = 0.03$ . When we compare all the experiments, it is apparent that the experiments with an initial deoxidant of  $[\text{pct Mg}]_i = 0.03$  contained the highest number of inclusions in the range of 1 to 2  $\mu\text{m}$ , and in the case with an initial deoxidant of  $[\text{pct Mg}]_i = 0.1$ , there were the most inclusions in nanoscale. In addition, the inclusions with 10  $\mu\text{m}$  and even larger were observed in Exp. A1 and Exp. A2M1.

The experiments with the amount of initial deoxidant  $[\text{pct Al}]_i = 0.25$  pct were chosen to study the change of inclusion size distribution with the holding time at 1873 K (1600 °C). As shown in Figure 6, the curves tend to be broader and lower with the holding time, indicating that the inclusion size increases and the number of inclusions decreases with the increasing holding time. Furthermore, the number of inclusions in the experiment with an initial deoxidant amount of  $[\text{pct Mg}]_i = 0.1$  was extremely large despite no information about inclusions smaller than 200 nm and the shape of curve at 120 seconds indicates there were lots of inclusion in nanoscale.

### 2. Number and size of three-dimensional inclusions

Figure 7 depicts the effect of Mg addition on number and average diameter of three-dimensional inclusions at holding time of 3900 seconds at 1873 K (1600 °C). It is clear that the number of inclusions in the Al and Mg complex deoxidation was higher, as compared with those in Al-only addition experiments, and it was higher relatively in the experiments with an initial deoxidant of  $[\text{pct Mg}]_i = 0.03$ . In addition, the inclusion number increases with the decrease of the Al content. The variation of the average diameter of inclusions shows that with the increasing amount of Mg and Al addition, the average diameter of inclusions decreases significantly.

The change of inclusion number and average diameter is shown in Figure 8, as a function of holding time. It is found that the number of inclusions decreases and the inclusion size increases greatly during the first 1800 seconds after deoxidation. Due to the underestimation of small inclusions in A2-2 as shown in Figure 6, the number of inclusions should be more than  $14 \times 10^8 \text{ cm}^{-3}$ . Combined with the volume fraction of inclusions shown in Table II, the ascending velocity of inclusions is lowest in Exp. A2M1. Furthermore, the slope of curves in Figure 8 implies the coarsening rate decreases with the holding time and increases in the order of A2-2, A2-1, A2 at the early stage of deoxidation.

### C. Homogeneity of Inclusion Dispersion

To observe the homogeneity of inclusion dispersion in the steel directly, the area density of inclusions on the cross section at 3900 seconds after deoxidation was analyzed as displayed in Figure 9, which was obtained by measuring the area of inclusion sections on each

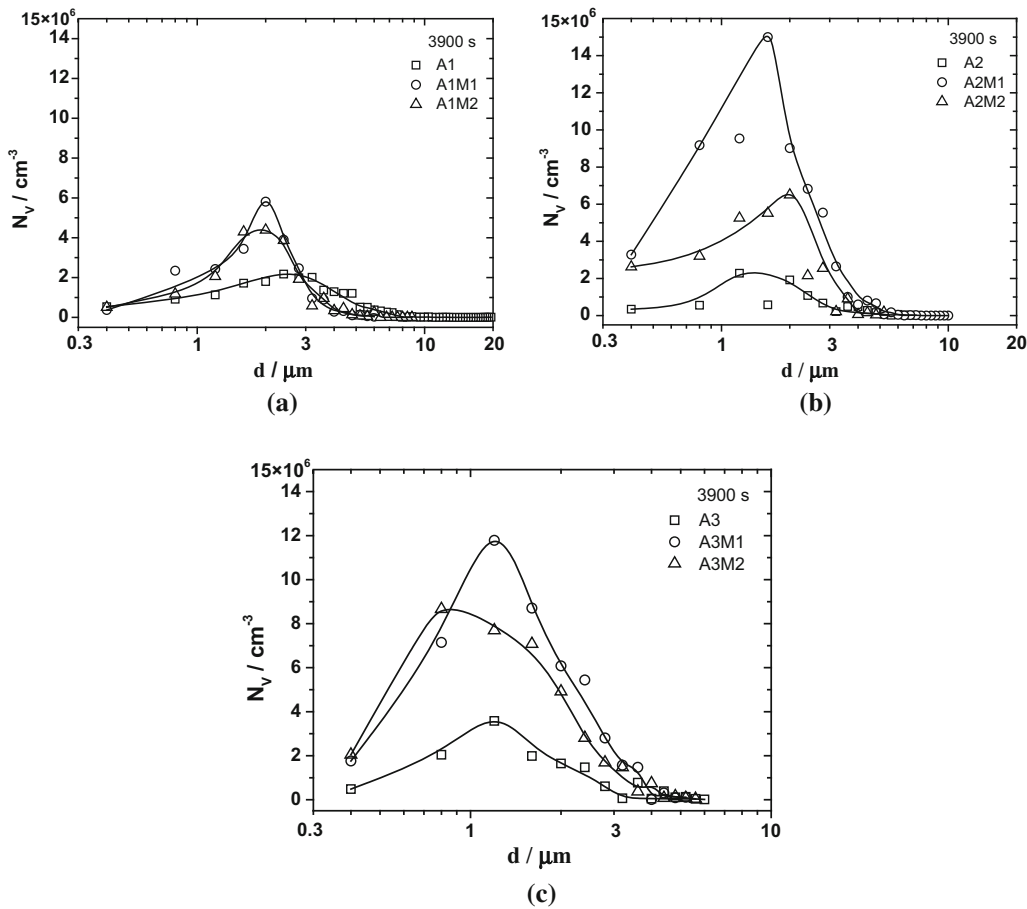


Fig. 5—Effect of Mg addition on the size distribution of three-dimensional inclusions in the steel with different Al contents: (a) [pct Al]<sub>i</sub> = 0.05 pct, (b) [pct Al]<sub>i</sub> = 0.25 pct, and (c) [pct Al]<sub>i</sub> = 0.55 pct.

SEM microphotograph (one SEM microphotograph corresponding to the actual observed area of 0.073 mm<sup>2</sup>). It can be seen that the inclusions dispersed nonuniformly in Exp. A1, Exp. A2M1, and Exp. A3M1, where the volume fraction of inclusion was large and the average MgO content of inclusion was less than 16 pct. The inclusions segregated in a certain area in Exp. A1 in which the largest area density of inclusions accounted for 1.6 to 3.2 pct. In the case of Al ([pct Al]<sub>i</sub> = 0.25) and Mg ([pct Mg]<sub>i</sub> = 0.03) deoxidation, the segregated region of inclusions was large enough to about one third of the total observed area. Furthermore, it is found that the large inclusions detected in Exp. A1 and Exp. A2M1 as shown in Figure 6 may due to the sintering of segregated inclusions.

To analyze the factors affecting the inclusion distribution, it is necessary to quantify the homogeneity in inclusion dispersion. As the area density of inclusions is affected by not only the number of inclusions but also the inclusion size, the intersurface distance was measured to describe the degree of homogeneity in inclusion dispersion. A mean minimum intersurface distance of all inclusions on each SEM microphotograph was calculated  $D_{mk}$  is the mean value of  $D_{mi}$  for each SEM microphotograph and degree of homogeneity in

inclusion dispersion  $H$  is defined as the reciprocal of the relative standard deviation of  $D_{mk}$ :

$$H = \frac{\overline{D_A}}{\sqrt{\frac{\sum_{i=1}^n (D_{mk} - \overline{D_A})^2}{n-1}}} \quad [8]$$

where  $\overline{D_A}$  is the arithmetic mean value of  $D_{mk}$  and the value of  $n$  is 169 or 338 in this article. The effect of Mg addition on degree of homogeneity in inclusion dispersion at 3900 seconds was shown in Figure 10, which agrees well with the results in Figure 9 and the total oxygen content. It is found that the change of degree of homogeneity in inclusion dispersion is not regular with the increasing Mg addition but with the inclusion composition. The degree of homogeneity in inclusion dispersion increases in the order, groups with inclusions containing Al<sub>2</sub>O<sub>3</sub> + spinel ([pct Mg]<sub>i</sub> = 9500072881 0.03, [pct Al]<sub>i</sub> = 0.25 or 0.55), groups with inclusions containing isolated spinel-only ([pct Mg]<sub>i</sub> = 0.03, [pct Al]<sub>i</sub> = 0.05; [pct Mg]<sub>i</sub> = 0.1, [pct Al]<sub>i</sub> = 0.25 or 0.55), groups with inclusions containing spinel + MgO ([pct Mg]<sub>i</sub> = 0.1, [pct Al]<sub>i</sub> = 0.05), and increases with Al content. These results indicate that the degree of homogeneity in inclusion dispersion is

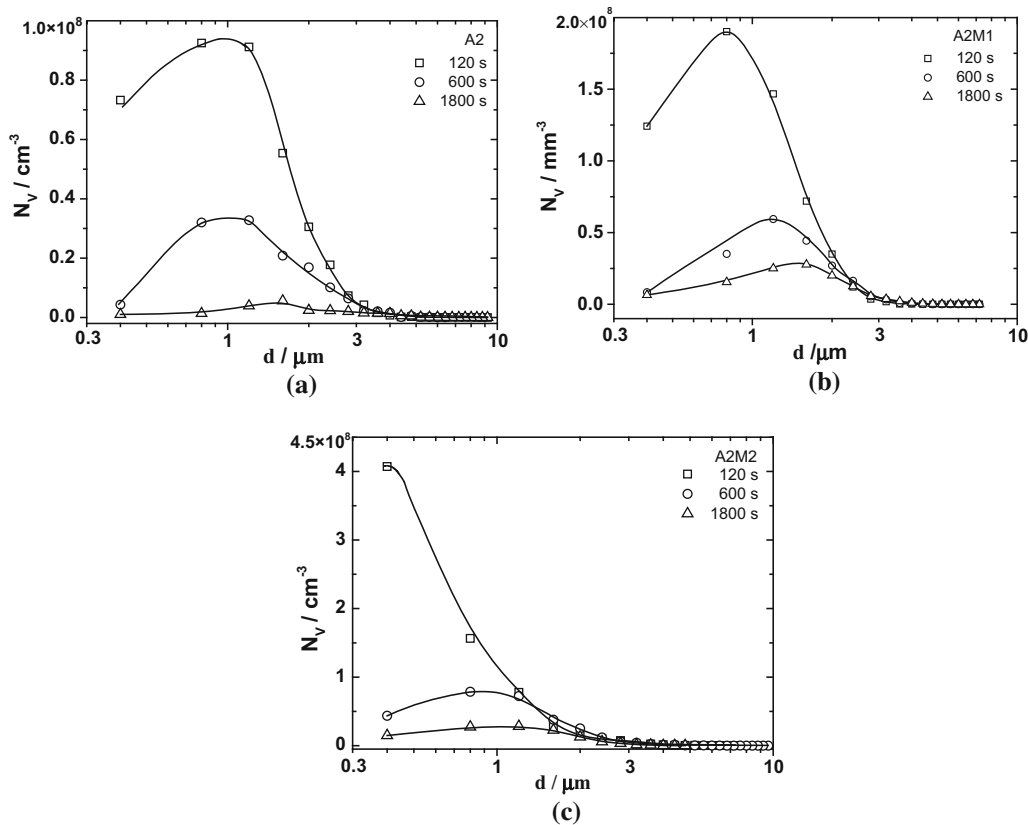


Fig. 6—Change of inclusion size distribution with holding time: (a) [pct Al]<sub>i</sub> = 0.25 pct, (b) [pct Al]<sub>i</sub> = 0.25 pct, [pct Mg]<sub>i</sub> = 0.03 pct, and (c) [pct Al]<sub>i</sub> = 0.25 pct, [pct Mg]<sub>i</sub> = 0.1 pct.

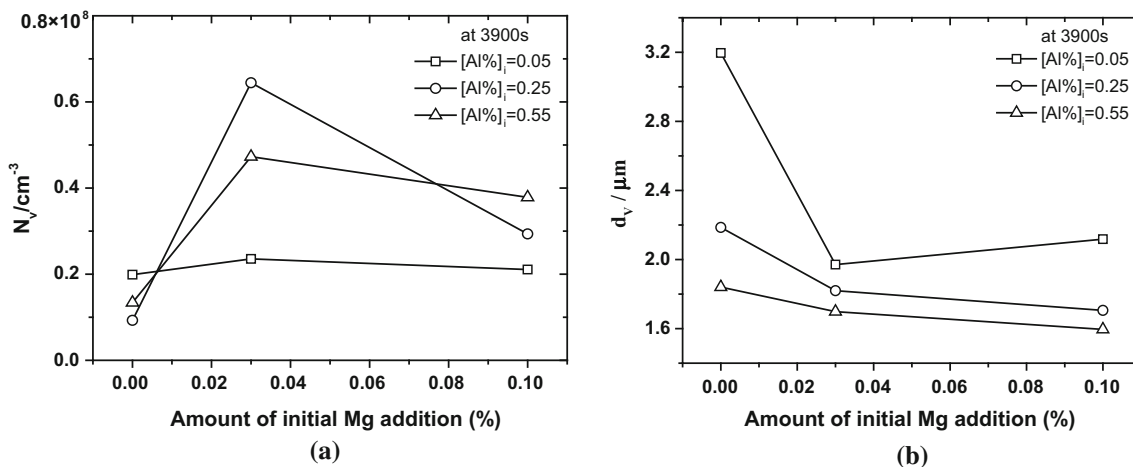


Fig. 7—Effect of Mg addition on the number and average diameter of three-dimensional inclusions: (a) number and (b) average diameter.

largely dependent on the composition and volume fraction of inclusions.

As shown in Figure 11, the degree of homogeneity in inclusion dispersion changed differently with holding time in Exp. A2, Exp. A2M1, and Exp. A2M2. To obtain homogenized distribution inclusions, the holding time was expected to be more than 1800 seconds in Exp. A2M2.

#### IV. DISCUSSION

##### A. Nucleation of Inclusions in Deoxidation

Based on classic homogeneous nucleation theory, the critical size of nuclei,<sup>[32]</sup>  $r_c$ , is given by:

$$r_c = -\frac{2\gamma_{SL}}{\Delta G_V} = \frac{2\gamma_{SL} \cdot V_O}{RT \ln S_O} \quad [9]$$

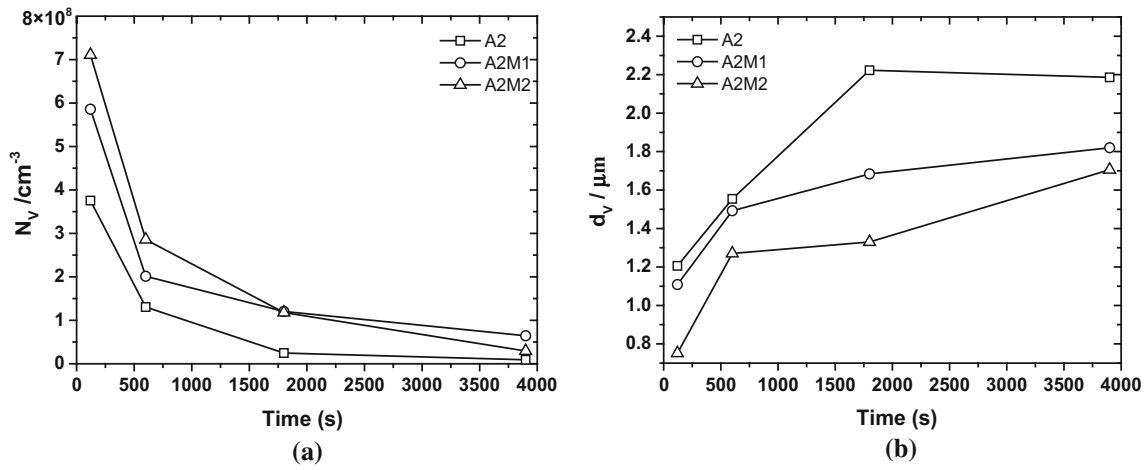


Fig. 8—Change of inclusion number and average diameter with holding time: (a) number and (b) average diameter.

where  $V_O$  is the molar volume of oxide ( $\text{m}^3/\text{mol}$ ) and  $S_O$  is the supersaturation degree.  $R$  is the gas constant ( $\text{J mol}^{-1} \text{K}$ ), and  $T$  is the absolute temperature ( $\text{K}$ ).  $\gamma_{\text{SL}}$  is the interfacial energy between oxide and liquid steel ( $\text{J/m}^2$ ), and it can be estimated as the following relationship:

$$\gamma_{\text{SL}} = \gamma_{\text{SV}} - \gamma_{\text{LV}} \cos \theta \quad [10]$$

$$\gamma_{\text{LV}} = \gamma_o - \sum \gamma_{\text{Fe}}^i \quad [11]$$

$$\gamma_o = 2.858 - 0.0051T \quad [12]$$

where  $\gamma_{\text{SV}}$  is the surface energy of solid inclusion,  $\gamma_{\text{LV}}$  is the surface energy of the liquid steel,  $\theta$  is the contact angle of liquid steel on solid oxide,  $\gamma_o$  is the surface energy of pure liquid iron, and  $\gamma_{\text{Fe}}^i$  is the effect of steel composition on the surface energy of the liquid steel. On substituting the relevant data in Table I, Table III, and Eq. [12] into Eq. [11], the following relationship is derived:<sup>[47]</sup>

$$\gamma_{\text{LV}} = 1.75 - 0.279 \ln(1 + 140 \cdot a_o) \quad [13]$$

The nucleation rate,<sup>[32]</sup>  $I$  ( $\text{cm}^{-3} \text{s}^{-1}$ ), can be obtained by:

$$\ln I = \frac{16\pi\gamma_{\text{SL}}^3 V_O^2}{3k_B R^2 T^3} \left( \frac{1}{(\ln S_O^*)^2} - \frac{1}{(\ln S_O)^2} \right) \quad [14]$$

where  $S_O^*$  is the critical supersaturation degree, which is value of  $S_O$  at  $I = 1$  ( $\text{cm}^{-3} \text{s}^{-1}$ ) and  $k_B$  is the Boltzmann constant ( $1.38 \times 10^{-23} \text{ J K}^{-1}$ ).

The calculated critical size of nuclei and nucleation rate for oxide inclusions at 1873 K (1600 °C) are shown in Figure 12 (Table IV and V), indicating that there is little difference in the critical size of the nucleus for  $\text{Al}_2\text{O}_3$ ,  $\text{MgAl}_2\text{O}_4$ , and  $\text{MgO}$ , which are in the range of

0.1 to 2 nm. It can be said that the nucleation rate is strongly dependent on the activity of oxygen when  $a_o$  exceeds a certain value and the nucleation rate for  $\text{Al}_2\text{O}_3$ , and  $\text{MgAl}_2\text{O}_4$  increases with the increasing  $a_o$ . In addition, the nucleation rate for  $\text{MgO}$  increases first and then decreases with the increasing oxygen activity, and  $\ln I$  for  $\text{MgO}$  reaches the maximum about 1860 when  $a_o$  is 100 ppm.

The composition of steels was estimated without considering the effect of dissolution and diffusion rate of deoxidants as listed in Table VII, and the activity was calculated by substituting relevant data in Tables VI and VII to Wagner equation. The estimated results for experimental samples in Figure 12 indicate that  $a_o$  is affected by the content of Al in the case with the same initial oxygen, and hence, decreasing Al addition appropriately is conducive to the increase of the nucleation rate. The total volume fraction of nucleuses in Exp. A2, Exp. A2M1, and Exp. A2M2 can be estimated based on the volume fraction of inclusions at 120 seconds and oxygen change during the first 120 seconds of deoxidation (the volume fraction of inclusions floating up to the surface of steel can be estimated by substituting the decreased amount of oxygen content in Tables II and VII into Eq. [1]). The experimental nucleation rate can be calculated by Eq. [15]. According to the study of Lindberg,<sup>[55]</sup> Miyashita,<sup>[56]</sup> and G. Li,<sup>[57]</sup> the dissolved O content decreased sharply and the deoxidation equilibrium establishes in a short time. The average nucleation rate in Exp. A2, Exp. A2M1, and Exp. A2M2 was estimated by considering the time for equilibrium of nucleus volume was 0.2 seconds based on the report of Lindberg.<sup>[55]</sup> It can be seen in Table VII that the average nucleation rate increased in the order of Exp. A2, Exp. A2M1, and Exp. A2M2, indicating a same change trend with theoretical calculated results in Figure 12, and that the nucleation rate increases with the increasing amount of Mg addition:

$$\bar{I} = \frac{f_V}{\frac{4}{3}\pi r_C^3 \cdot t} \quad [15]$$



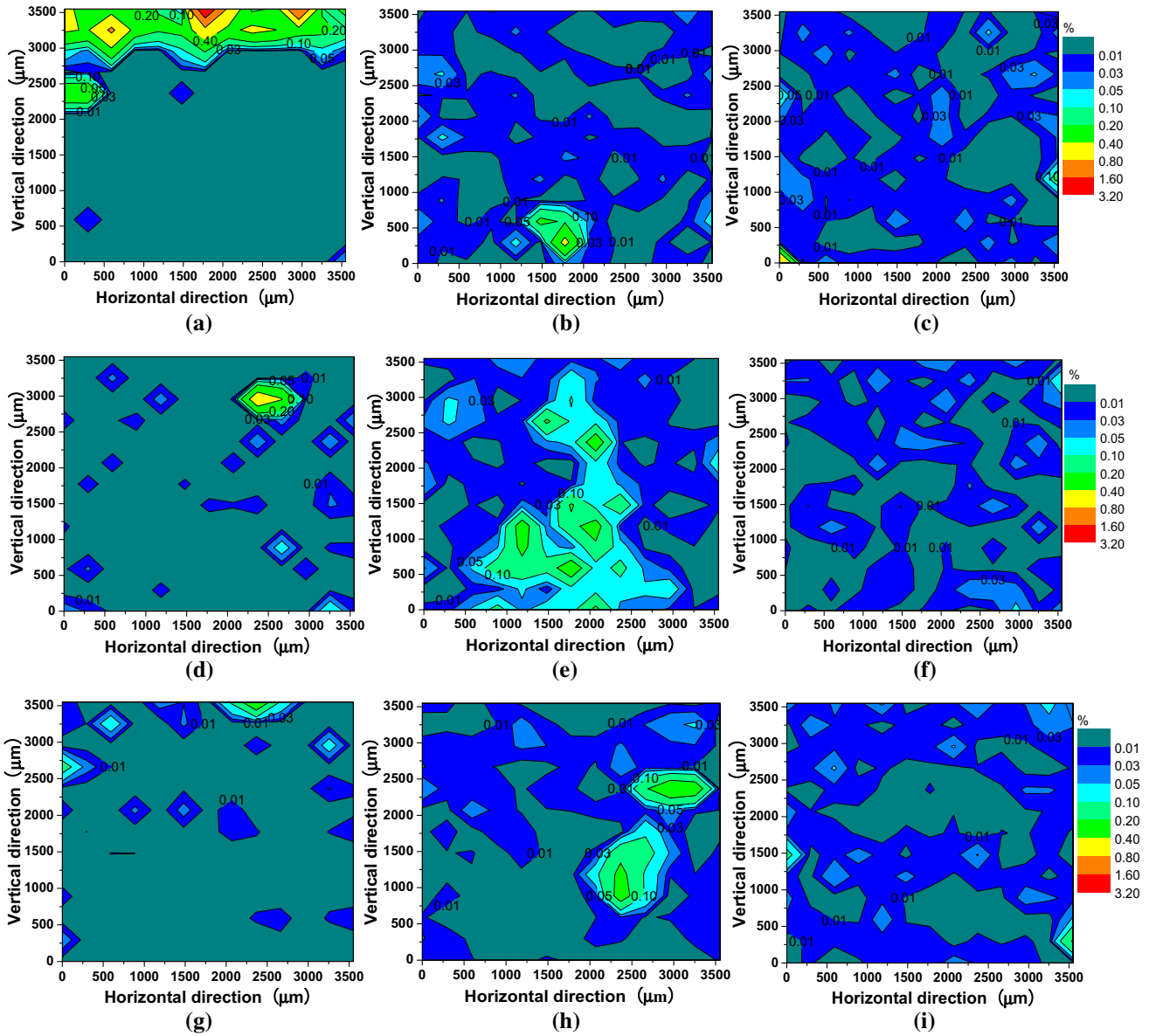


Fig. 9—Density distribution of inclusions on the cross section at 3900 s: (a) [pct Al]<sub>i</sub> = 0.05, (b) [pct Al]<sub>i</sub> = 0.05, [pct Mg]<sub>i</sub> = 0.03, (c) [pct Al]<sub>i</sub> = 0.05, [pct Mg]<sub>i</sub> = 0.1, (d) [pct Al]<sub>i</sub> = 0.25, (e) [pct Al]<sub>i</sub> = 0.25, [pct Mg]<sub>i</sub> = 0.03, (f) [pct Al]<sub>i</sub> = 0.25, [pct Mg]<sub>i</sub> = 0.1 (g) [pct Al]<sub>i</sub> = 0.55, (h) [pct Al]<sub>i</sub> = 0.55, [pct Mg]<sub>i</sub> = 0.03, and (i) [pct Al]<sub>i</sub> = 0.55, [pct Mg]<sub>i</sub> = 0.1.

### B. Growth of Inclusions in the Deoxidant

Based on the research of Ohta,<sup>[31]</sup> the particle growth by Ostwald ripening can be expressed by:

$$\bar{r}^3 - \bar{r}_0^3 = k_s \cdot t \quad [16]$$

$$k_s = k_d \cdot \alpha \quad [17]$$

with  $k_d$  as:

$$k_d = \frac{2\gamma D_O V_O C_O}{RT(C_P - C_O)} \quad [18]$$

where  $\bar{r}$  and  $\bar{r}_0$  is the mean particle radius at time  $t$  (m) and that at the start of Ostwald growth (m),  $\alpha$  is the

coarsening coefficient ( $\alpha = 0.47$  in LSW theory and  $\alpha = 0.754f_v^{1/3}$  from communicating neighbor (CN) model<sup>[31]</sup>),  $D_O$  is the diffusion constant of oxygen ( $2.91 \times 10^{-9} \text{ m}^2 \text{ s}^{-1}$ ),  $C_O$  is the dissolved oxygen concentration expressed by weight per unit volume ( $\text{kg m}^{-3}$ ), and  $C_P$  is the oxygen concentration in oxide expressed by weight per unit volume ( $\text{kg m}^{-3}$ ).

The  $k_s$  values for each experiment were calculated and plotted as the observed values in Figure 13. It can be seen that the change trend of  $k_{s(\text{cal.})}$  from these two ways corresponds to  $k_{s(\text{obs.})}$ , but LSW theory is more applicable in which  $\alpha$  is 0.47.

As  $\alpha$  is a constant, the coarsening rate  $k_s$  is proportional to  $k_d$ . The value of  $k_d$  is plotted as a function of oxygen content and amount of Mg addition in Figure 14, suggesting that the value of  $k_d$  is mainly

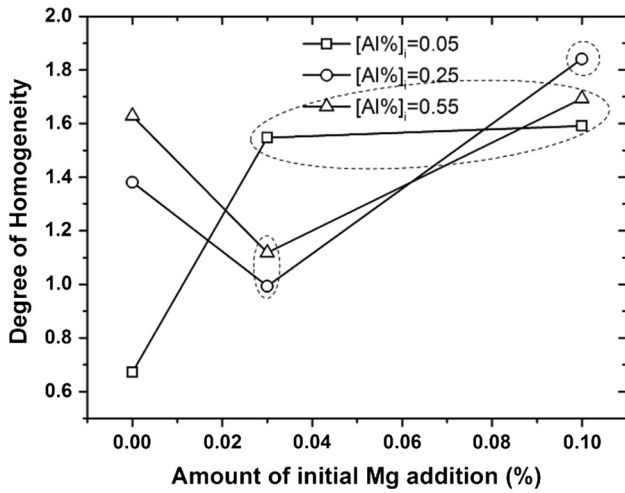


Fig. 10—Effect of Mg addition on degree of homogeneity in inclusion dispersion at 3900 s.

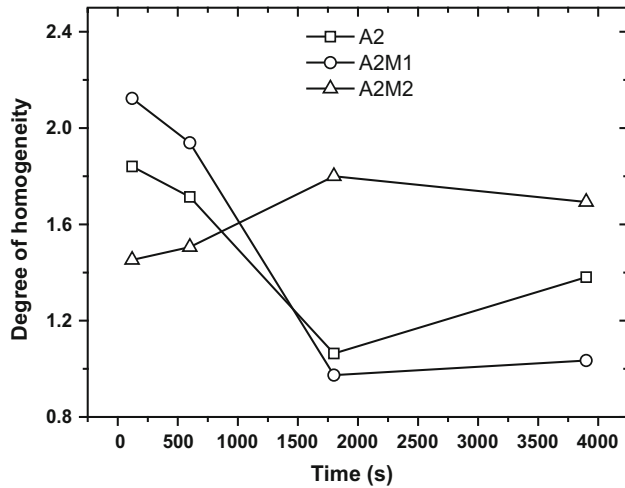


Fig. 11—Change of degree of homogeneity in inclusion dispersion with holding time.

dependent on the dissolved oxygen content and increases with the increasing oxygen content. Combined with the results of nucleation rate in Figure 12, the control of oxygen content has a strong influence on the size and number of inclusions. Therefore, increasing the oxygen activity at an early stage of deoxidation and lowering the dissolved oxygen content promote the formation of numerous fine inclusions.

The steel composition affected by Mg addition at equilibrium is calculated by FACTSAGE 7.0, as shown in Figure 14(b), indicating that increasing the Mg addition is favorable to the refinement of inclusions. Furthermore, when the initial Mg addition is 0.0040 and 0.0100 pct, the value of  $k_d$  decreases significantly.

### C. Attractive Force Acted on Inclusions

According to Paunov's theory,<sup>[24]</sup> the average attractive force acted on inclusions in the experiment was estimated with the measurement of minimum intersurface distance of inclusions and is plotted in Figure 15 with degree of homogeneity in inclusion dispersion. The reasonable size range of inclusions by using Paunov's theory in this study is  $d < 46 \mu\text{m}$ . The change trend of data indicates that the degree of homogeneity of inclusion distribution decreases with the increasing attractive force; *i.e.*, the inclusions disperse uniformly in the steel when the attractive force between inclusions is small. There are some deviation of data probably due to the error in estimation of attractive force without considering the effect of MgO content on the contact angle between spinel and molten steel.

As shown in Figure 16, the attractive force acted on inclusions decreases with the increasing MgO content and the decreasing volume fraction of inclusions, and this is the reason that the inclusions dispersed nonuniformly in Exp. A1, Exp. A2M1, and Exp. A3M1. Moreover, it can be explained that the highest number of inclusions left in the experiments with an initial

Table III. Effect of Steel Composition on Surface Energy of Liquid Steel ( $\text{J}/\text{m}^2$ )

Element	C	Si	Mn	P	N	Al
$\gamma_{\text{Fe}}^i$	$0.065[\text{C pct}]^{[45]}$	$0.026[\text{Si pct}]^{[46]}$	$0.050[\text{Mn pct}]^{[46]}$	$0.025[\text{P pct}]^{[46]}$	$5.585[\text{N pct}]^{[46]}$	$0.037[\text{Al pct}]^{[46]}$
Element	Cr	Cu	Ni	S	O	
$\gamma_{\text{Fe}}^i$	$0.008[\text{Cr pct}]^{[46]}$	$0.026[\text{Cu pct}]^{[46]}$	$0.002[\text{Ni pct}]^{[46]}$	$0.2\ln(1 + 330[\text{pct S}])^{[47]}$	$0.279\ln(1 + 140[a_{\text{O}}])^{[48]}$	

Table IV. Parameters Used in the Calculation of Critical Size of Nuclei and Nucleation Rate

Oxide	Oxides/Fe at 1873 K (1600 °C) $\theta$ (deg)	$\gamma_{\text{SV}}$ ( $\text{J}/\text{m}^2$ )	$V_0$ ( $\text{m}^3/\text{mol}$ )
$\text{Al}_2\text{O}_3$	$132 - 6.3\ln(1 + 400[\text{pct O}]) - 0.63\ln(1 + 640[\text{pct S}])^{[47]}$	$1.128 - 0.0001T^{[48]}$	$8.6 \times 10^{-6}$
MgO	$117 - 7.4\ln(1 + 1720a_{\text{O}})(-15 < \text{Log}a_{\text{O}} < -9)^{[49]}$	$0.86^{[50]}$	$11 \times 10^{-6}$
$\text{MgAl}_2\text{O}_4$	$105^{[51]}$	$2.270 - 0.0006T^{[52,53]}$	$9.3 \times 10^{-6}$

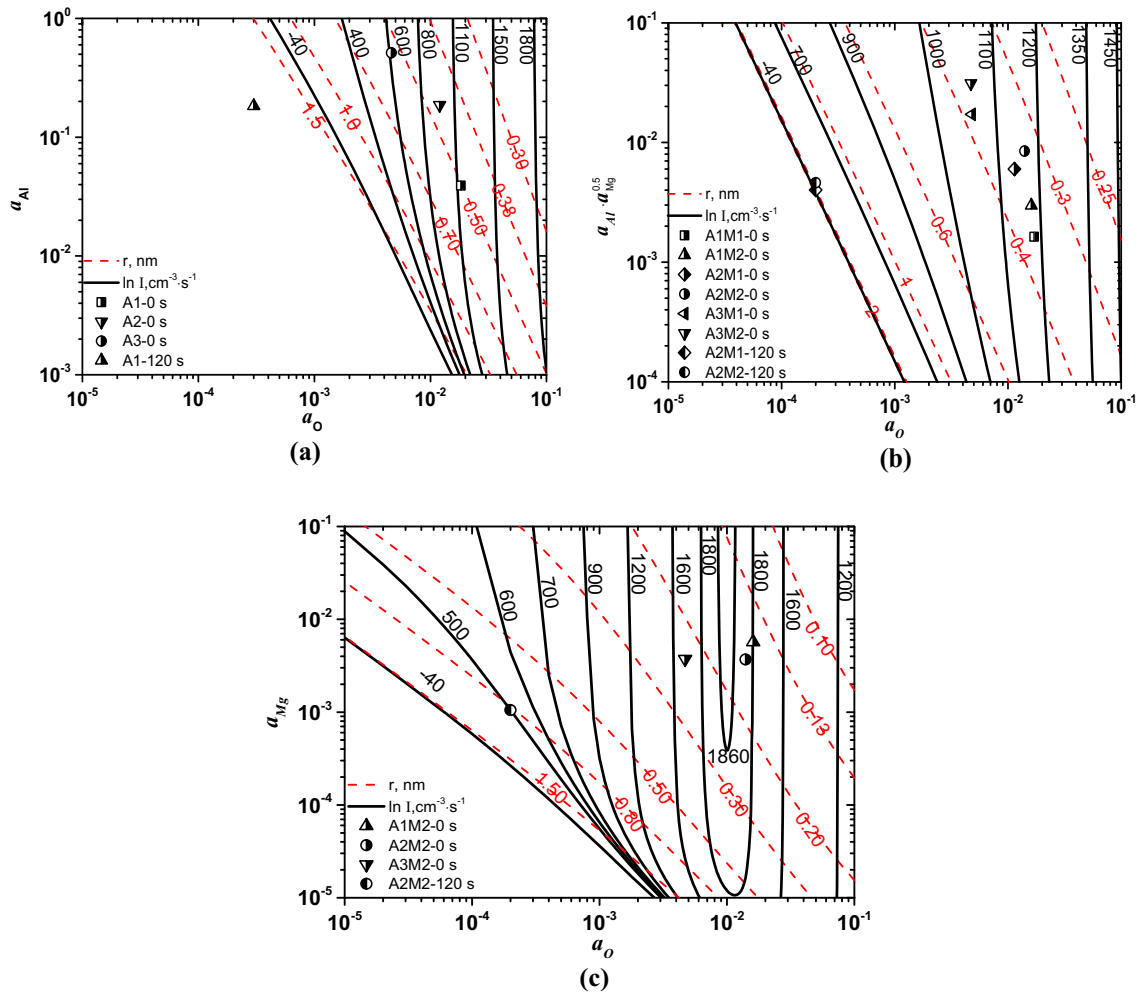


Fig. 12—Calculated critical size of nuclei and nucleation rate for oxide inclusions at 1873 K (1600 °C): (a)  $\text{Al}_2\text{O}_3$ , (b)  $\text{MgAl}_2\text{O}_4$ , and (c)  $\text{MgO}$ .

Table V. Equilibrium Constants Used in this Study

Reaction	$\log K_{\text{eq}}$
$\text{Al}_2\text{O}_3(\text{s}) = 2[\text{Al}] + 3[\text{O}]$	$-12.57 = (-45300/T + 11.62)^{[54]}$
$\text{MgO}(\text{s}) = [\text{Mg}] + [\text{O}]$	$-7.86 = (-38059/T + 12.45)^{[54]}$
$\text{MgAl}_2\text{O}_4(\text{s}) = [\text{Mg}] + 2[\text{Al}] + 4[\text{O}]$	$-21.28 = (-84339/T + 23.75)^{[54]}$

Table VI. Interaction Coefficients of O, Al, and Mg at 1873 K (1600 °C)

$e_i^j(\rightarrow j)$	C	Si	Mn	P	S	Cr	Cu	Ni	Ti	N	O	Al	Mg
O	-0.42	-0.066	-0.021	0.070	-0.13	-0.055	-0.013	0.006	-0.34	-0.14	-0.17	-1.17	-1.98
Al	0.091	0.056	-0.004	0.033	0.035	0.012	-0.013	-0.017		0.015	-1.98	0.043	-0.13
Mg	-0.31	-0.088				0.047		-0.012	-0.64		-3	-0.12	

deoxidant of  $[\text{pct Mg}]_i = 0.03$  is due to the large attractive force and low buoyancy acted on inclusions (buoyancy decreases with a decrease of size and density of inclusion).

## V. SUMMARY AND CONCLUSION

In the experiments of the steel deoxidized with different contents of aluminum and magnesium under the condition of no fluid flow at 1873 K (1600 °C), the

**Table VII. Estimated Composition of Steels Before Deoxidation and Nucleation Rate (Weight Percent)**

Composition	[O]	[Al]	[Mg]	$a_0$	$a_{Al}$	$a_{Mg}$	$\bar{I}, \text{cm}^{-3} \text{s}^{-1}$
A1	0.0208	0.0428	0	0.018272	0.03915	0	—
A1M1	0.0195	0.0428	0.002	0.016983	0.039359	0.001722	—
A1M2	0.0189	0.0428	0.0066	0.016123	0.039412	0.005706	—
A2	0.0214	0.2274	0.001	0.011378	0.211198	0.000808	$1.02 \times 10^{19}$
A2M1	0.0209	0.2011	0	0.011985	0.186767	0	$2.06 \times 10^{19}$
A2M2	0.0219	0.1518	0.0045	0.014046	0.139469	0.003698	$2.09 \times 10^{20}$
A3	0.0197	0.533	0	0.004622	0.514347	0	—
A3M1	0.0204	0.533	0.0015	0.004753	0.512479	0.001121	—
A3M2	0.0206	0.533	0.005	0.004723	0.511476	0.003731	—

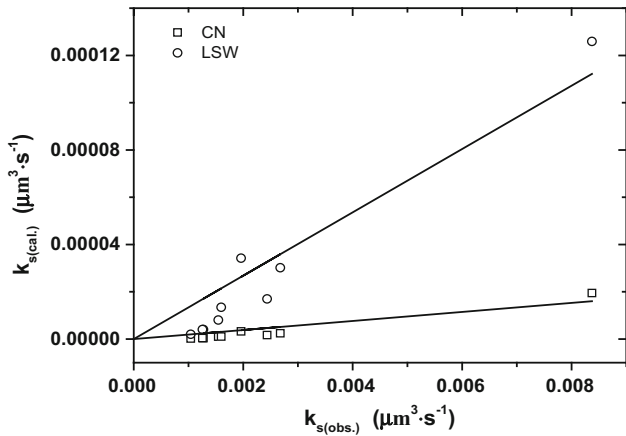


Fig. 13—Comparison of  $k_{s(\text{cal})}$  from Ostwald growth and  $k_{s(\text{obs.})}$  from inclusion size.

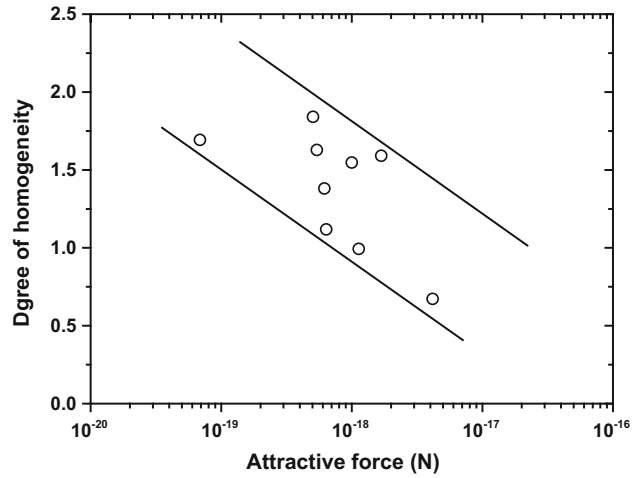


Fig. 15—Relationship between degree of homogeneity and attractive force.

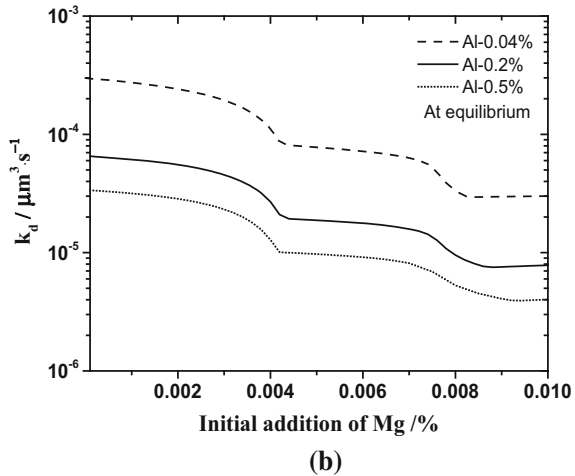
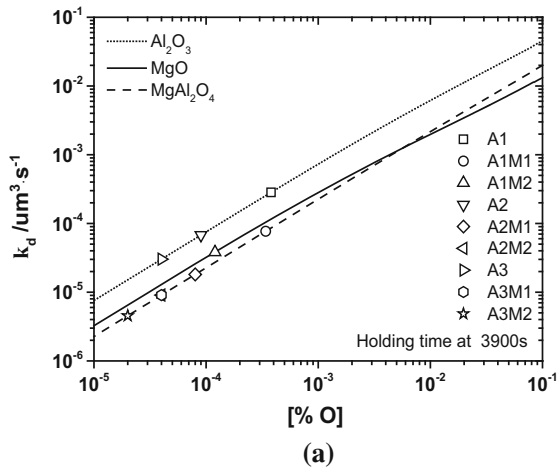


Fig. 14—Relationship between  $k_d$  with oxygen content and amount of Mg addition for  $\text{Al}_2\text{O}_3$ ,  $\text{Al}_2\text{O}_3$ -MgO, and MgO: (a) oxygen content and (b) Mg addition.

effect of Mg addition on the refinement and homogenized distribution of inclusions has been studied systematically by the measurement of the composition, size, number, area density of inclusions, degree of homogeneity in inclusion dispersion, and the estimation of the nucleation, coarsening, and attractive force of  $\text{Al}_2\text{O}_3$ ,

$\text{MgAl}_2\text{O}_4$ , and MgO inclusions. The main findings are summarized as follows:

1. Experimental results about the size and number of inclusions indicate that numerous fine inclusions precipitated in the steel with Mg addition at 1873 K

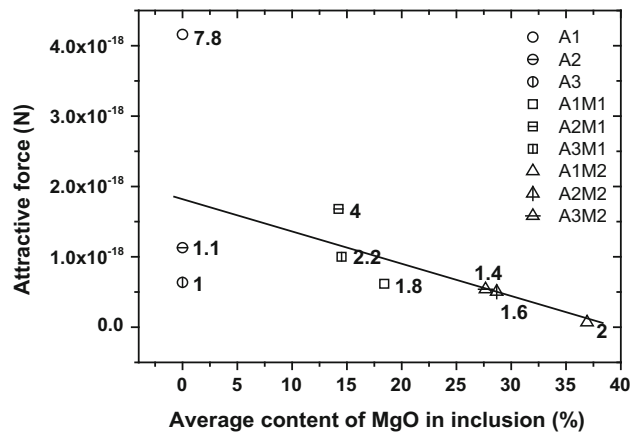


Fig. 16—Relationship between attractive force and the composition of inclusions (the volume fraction of inclusions ( $10^{-4}$ ) is marked on the figure).

- (1600 °C) and there were still a large number of inclusions in the range of 1 to 2  $\mu\text{m}$  and nanoscale left in the experiments with initial deoxidants of  $[\text{pct Mg}]_i = 0.03$  and  $[\text{pct Mg}]_i = 0.1$ , respectively. The number of inclusions was highest in the experiments with an initial deoxidant of  $[\text{pct Mg}]_i = 0.03$ , and the average diameter of inclusions decreases generally with the increasing amount of Mg and Al addition at 3900 seconds after deoxidation. In addition, it is found that the number of inclusions decreases and the inclusion size increases significantly during the first 1800 seconds after deoxidation.
- Experimental results about the dispersion of inclusions show that the inclusions dispersed nonuniformly in the steel where the volume fraction of inclusions was large and the average MgO content of inclusions was less than 16 pct. The degree of homogeneity in inclusion dispersion increases in the order, groups with inclusions containing  $\text{Al}_2\text{O}_3$  + spinel ( $[\text{pct Mg}]_i = 0.03$ ,  $[\text{pct Al}]_i = 0.25$  or  $0.55$ ), groups with inclusions containing isolated spinel-only ( $[\text{pct Mg}]_i = 0.03$ ,  $[\text{pct Al}]_i = 0.05$ ;  $[\text{pct Mg}]_i = 0.1$ ,  $[\text{pct Al}]_i = 0.25$  or  $0.55$ ), and groups with inclusions containing spinel + MgO ( $[\text{pct Mg}]_i = 0.1$ ,  $[\text{pct Al}]_i = 0.05$ ). In addition, to obtain homogenized distribution inclusions, the holding time was expected to be more than 1800 seconds in Exp. A2M2.
  - The estimation of nucleation and coarsening of inclusions corresponds to the experimental results, and it is found that increasing the oxygen activity at an early stage of deoxidation and lowering the dissolved oxygen content promote the formation of numerous fine inclusions. Furthermore, increasing the initial Mg addition is conducive to the increase of the nucleation rate as well as to the refinement of the inclusion.
  - The calculated average attractive force of inclusions in experimental steels according to Paunov's theory indicates that the degree of homogeneity in  $\text{Al}_2\text{O}_3$ -MgO inclusion dispersion decreases with an increase of attractive force acted on inclusions, which

decreases with the increasing MgO content and decreasing volume fraction of inclusions.

## ACKNOWLEDGMENT

This research is supported by the National Science Foundation of China (Nos. 51574190 and 51574020) and the Open Fund of State Key Laboratory of Advanced Metallurgy (Grant No. KF14-02 and KF14-06).

## REFERENCES

- P. Kaushik, J. Lehmann, and M. Nadif: *Metall. Mater. Trans. B*, 2012, vol. 43B, pp. 710–25.
- S. Beretta and Y. Murakami: *Metall. Mater. Trans. B*, 2001, vol. 32B, pp. 517–23.
- P. Juvonen: Master's Thesis, Helsinki University of Technology, 2004.
- G.N. Shannon and S. Sridhar: *High Temp. Mater. Process.*, vol. 24, pp. 111–24.
- S. Sridhar and A.W. Cramb: *High Temp. Mater. Process.*, 2003, vol. 22, pp. 275–82.
- S. Sridhar and A.W. Cramb: *Metall. Mater. Trans. B*, 2000, vol. 31B, pp. 406–10.
- L. Wang, S. Yang, J. Li, T. Wu, W. Liu, and J. Xiong: *Metall. Mater. Trans. B*, 2016, vol. 47B, pp. 99–107.
- P.C. Pistorius and N. Verma: *Microsc. Microanal.*, 2011, vol. 17, pp. 963–71.
- L. Zhang and B.G. Thomas: *ISIJ Int.*, 2003, vol. 43, pp. 271–91.
- D.S. Sarma, A.V. Karasev, and P.G. Jönsson: *ISIJ Int.*, 2009, vol. 49, pp. 1063–74.
- F. Ishikawa, T. Takahashi, and T. Ochi: *Metall. Mater. Trans. A*, 1994, vol. 25, pp. 929–36.
- K. Hashimoto, T. Fujimatsu, N. Tsunekage, K. Hiraoka, K. Kida, and E.C. Santos: *Mater. Des.*, 2011, vol. 32, pp. 1605–11.
- T.B. Braun, J.F. Elliott, and M.C. Flemings: *Metall. Trans. B*, 1979, vol. 10, pp. 171–84.
- N. Verma, P.C. Pistorius, R.J. Fruehan, M.S. Potter, H.G. Oltmann, and E.B. Pretorius: *Metall. Mater. Trans. B*, 2012, vol. 43B, pp. 830–40.
- N. Verma, P.C. Pistorius, R.J. Fruehan, M.S. Potter, M. Lind, and S. Story: *Metall. Mater. Trans. B*, 2011, vol. 42B, pp. 711–19.
- N. Verma, P.C. Pistorius, R.J. Fruehan, M.S. Potter, M. Lind, and S. Story: *Metall. Mater. Trans. B*, 2011, vol. 42B, pp. 720–29.
- X. Wang, X. Li, Q. Li, F. Huang, H. Li, and J. Yang: *Steel Res. Int.*, 2014, vol. 85, pp. 155–63.
- G. Yang, X. Wang, F. Huang, P. Wei, and X. Hao: *Metall. Mater. Trans. B*, 2015, vol. 46B, pp. 145–54.
- Y. Miki and B.G. Thomas: *Metall. Mater. Trans. B*, 1999, vol. 30B, pp. 639–54.
- L. Zhang, S. Taniguchi, and K. Cai: *Metall. Mater. Trans. B*, 2000, vol. 31B, pp. 253–66.
- L. Zhang, J. Aoki, and B.G. Thomas: *Metall. Mater. Trans. B*, 2006, vol. 37B, pp. 361–79.
- X. Li, Y. Min, C. Liu, and M. Jiang: *Steel Res. Int.*, 2015, vol. 86, pp. 1530–40.
- R. Takata, J. Yang, and M. Kuwabara: *ISIJ Int.*, 2007, vol. 47, pp. 1379–86.
- S. Kimura, K. Nakajima, and S. Mizoguchi: *Metall. Mater. Trans. B*, 2001, vol. 32B, pp. 79–85.
- Z.H. Jiang, C. Wang, and W. Gong: *Ironmak. Steelmak.*, 2015, vol. 42, pp. 669–74.
- K. Isobe: *ISIJ Int.*, 2010, vol. 50, pp. 1972–80.
- K. Sakata and H. Suito: *Metall. Mater. Trans. B*, 1999, vol. 30B, pp. 1053–63.
- J.S. Park and J.H. Park: *Steel Res. Int.*, 2014, vol. 85, pp. 1303–9.
- L. Zhang and W. Pluschkell: *Ironmak. Steelmak.*, 2003, vol. 30, pp. 106–10.



30. J. Zhang and H.G. Lee: *ISIJ Int.*, 2004, vol. 44, pp. 1629–38.
31. H. Ohta and H. Suito: *ISIJ Int.*, 2006, vol. 46, pp. 42–9.
32. H. Suito and H. Ohta: *ISIJ Int.*, 2006, vol. 46, pp. 33–41.
33. H. Ohta and H. Suito: *ISIJ Int.*, 2006, vol. 46, pp. 14–21.
34. H. Ohta and H. Suito: *ISIJ Int.*, 2006, vol. 46, pp. 22–8.
35. K. Sakata and H. Suito: *Metall. Mater. Trans. B*, 1999, vol. 30B, pp. 1053–63.
36. M. Guo and H. Suito: *ISIJ Int.*, 1999, vol. 39, pp. 678–86.
37. H. Ohta and H. Suito: *Metall. Mater. Trans. B*, 1997, vol. 28B, pp. 1131–39.
38. L. Zhang, Y. Ren, H. Duan, W. Yang, and L. Sun: *Metall. Mater. Trans. B*, 2015, vol. 46B, pp. 1809–25.
39. H. Itoh, M. Hino, and S. Ban-Ya: *Metall. Mater. Trans. B*, 1997, vol. 28B, pp. 953–56.
40. S. Yang, Q. Wang, L. Zhang, J. Li, and K. Peaslee: *Metall. Mater. Trans. B*, 2012, vol. 43B, pp. 731–50.
41. J.H. Park and H. Todoroki: *ISIJ Int.*, 2010, vol. 50, pp. 1333–46.
42. S.A. Saltykov: *Stereology: Proceedings of the Second International Congress for Stereology*, H. Elias, ed., Springer, New York, 1967, p. 163.
43. T. Li, S. Shimasaki, S. Taniguchi, K. Uesugi, and S. Narita: *Metall. Mater. Trans. B*, 2013, vol. 44B, pp. 750–61.
44. I.H. Jung, S.A. Deckerov, and A.D. Pelton: *J. Phase Equilib. Diff.*, 2004, vol. 25, pp. 329–45.
45. I. Jimbo and A.W. Cramb: *ISIJ Int.*, 1992, vol. 32, pp. 26–35.
46. B.J. Keene: *Int. Mater. Rev.*, 1998, vol. 33, pp. 1–35.
47. D.R. Poirier, H. Yin, M. Suzuki, and T. Emi: *ISIJ Int.*, 1998, vol. 38 (3), pp. 229–38.
48. L. Zhao and V. Sahajwalla: *ISIJ Int.*, 2003, vol. 43, pp. 1–6.
49. H. Shibata, X. Jiang, M. Valdez, and A.W. Cramb: *Metall. Mater. Trans. B*, 2004, vol. 35B, pp. 179–81.
50. M. Humenik and W.D. Kingery: *J. Am. Ceram. Soc.*, 1954, vol. 31, pp. 18–23.
51. C.M. Fang, S.C. Parker, and G. De With: *J. Am. Ceram. Soc.*, 2000, vol. 83, pp. 2082–4.
52. H. Shibata, Y. Watanabe, K. Nakajima, and S.Y. Kitamura: *ISIJ Int.*, 2009, vol. 49, pp. 985–91.
53. R.H. Bruce: *Sci. Ceram.*, 1965, vol. 2, p. 359.
54. M. Hino and K. Ito: *Thermodynamic Data for Steelmaking*, 2nd ed., Tohoku University Press, Tohoku, 2010, pp. 247–64.
55. U. Lindberg and K. Torssel: *Trans. TMS-AIME.*, 1968, vol. 242, p. 94.
56. Y. Miyashita: *Tetsu-to-Hagané.*, 1966, vol. 52, p. 1049.
57. G. Li and H. Suito: *ISIJ Int.*, 1977, vol. 37, p. 762.